

Top of the Line Corrosion in H₂S/CO₂ Environments

Camacho A. *, Singer M., Brown B., Nesic S.
Ohio University - Institute for Corrosion and Multiphase Technology
342 West State Street, Athens, OH 45701

ABSTRACT

The objective of this research is to experimentally investigate the influence of H₂S on CO₂ on top of the line corrosion (TLC). Experiments were conducted in large scale multiphase flow loops at 3 bars absolute pressure and a fixed temperature of 70°C. Test duration ranged from 2 to 21 days. The tests were conducted on carbon steel coupons (API X-65), using deionized (DI) water as the electrolyte. It was found that the partial pressure of CO₂ and the partial pressure of H₂S have a strong effect on the general corrosion behavior at the top of the line. Moreover, the presence of trace amounts of H₂S seems to halt the tendency towards corrosion that is often observed under sweet conditions.

Keywords: top of the line corrosion, hydrogen sulfide, carbon dioxide.

INTRODUCTION

Carbon dioxide (CO₂) corrosion is the most prevalent form of attack encountered in oil and gas production; it is also a major concern in the application of carbon and low alloy steels. CO₂ corrosion phenomena have been widely studied¹⁻⁴. However, understanding and control of top of the line corrosion (TLC) lags significantly behind general understanding of CO₂ corrosion; this is particularly true when hydrogen sulfide (H₂S) is present.

*Present affiliation: Lloyd's Register Capstone Inc., 1505 Highway 6 South, Suite 100, Houston, TX 77077

Copyright

©2008 by NACE International. Requests for permission to publish this manuscript in any form, in part or in whole must be in writing to NACE International, Copyright Division, 1440 South creek Drive, Houston, Texas 777084. The material presented and the views expressed in this paper are solely those of the author(s) and are not necessarily endorsed by the Association. Printed in the U.S.A.

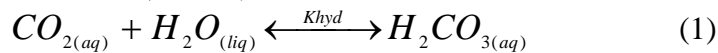
Top of the line corrosion occurs in multiphase flow or during wet gas transportation when water vapor condenses on the internal walls of the pipeline, due to the heat exchange occurring between the pipe and the surroundings. The condensed liquid then becomes enriched by the corrosive species present in the gas stream, such as carbon dioxide (CO₂) which yields carbonic acid (H₂CO₃) and hydrogen sulfide (H₂S).

Since TLC can happen only when water condensation occurs, it is often associated with failed thermal insulation. TLC is particularly problematic because it is difficult to ensure continuous inhibition in this case. In general one can distinguish three distinct corrosion regimes that can be found in a wet gas pipeline based on the location: bottom of the line corrosion, sidewall corrosion and at the top of the line corrosion⁵. The corrosive environment and conditions are considerably different at each of these locations. At the bottom of the line, the liquid is accumulated, the degradation is uniform and the corrosion rate can be lowered with the use of inhibitors. On the sidewalls of the pipe, where the condensed water drains to the bottom, the corrosion is also uniform, but the use of inhibitors is unreliable because it may be difficult for them to reach these locations. At the top of the line, the corrosion rate may be mitigated by a protective iron carbonate layer formation; however, continuous inhibition is virtually impossible; localized corrosion can occur if the corrosion layer does not offer uniform protection.

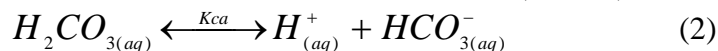
The main parameters influencing TLC are the temperature of the fluid, the CO₂ and H₂S partial pressures, the concentration of organic acids, the gas velocity and the condensation rate⁶⁻¹¹. General observations suggest that those parameters influence the corrosion rate (CR) in a complex way. At low condensation rates, a protective film of iron carbonate (FeCO₃) appears on the surface of the pipe, and this lowers the corrosion rate. The formation of this film is explained by the ferrous ion saturation of the liquid layer and precipitation of corrosion product⁶⁻¹¹. At high condensation rates, saturation cannot be reached, and the corrosion rate can remain high.

Concerns have been raised about the sour gas fields where TLC also may be a problem. The effect of small quantities of H₂S on TLC remains unknown to date. In the light of past TLC related failures of sour wet gas lines⁵, a better understanding of the H₂S effect on TLC is required.

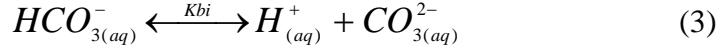
H₂S and CO₂ are “acid gases” which promote corrosion phenomena in gas transportation and production pipelines by the formation of weakly acidic species in water. At low pressure, the solubility of both H₂S and CO₂ can be estimated using Henry’s law. The difference in these two dissolved gases is that CO₂ must undergo a hydration reaction to form carbonic acid (H₂CO₃) before dissociation whereas aqueous H₂S is acidic and will directly dissociate once dissolved in the solution¹². Although there is no direct reaction between CO₂ and H₂S, the composition of the solution can be determined through a sequence of chemical reactions and by consideration of the effect of the H⁺ as a common ion. As CO₂ gas dissolves in water, aqueous CO₂ (CO_{2(aq)}) is hydrated to form carbonic acid (H₂CO₃).



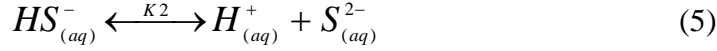
The H₂CO₃ dissociates to release a H⁺ and a bicarbonate ion (HCO₃⁻) in solution:



The HCO_3^- also dissociates to release another H^+ and a carbonate ion (CO_3^{2-}).

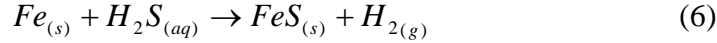


After H_2S dissolves in water, it dissociates to bisulfide (HS^-) and sulfide (S^{2-}) species in a series of dissociation reactions in solution:



Although H_2S gas is about three times more soluble than CO_2 gas, the acid created by dissociation of H_2S is about three times weaker than carbonic acid. Hence, the effect of H_2S gas on decreasing the solution pH is approximately the same as CO_2 gas¹³. The distribution of species is dependent upon the partial pressures of CO_2 and H_2S , temperature and pH. Species concentrations can be determined by solving the corresponding equilibrium reactions above.

Ignoring the metal cracking aspects associated with sour corrosion due to hydrogen permeation into the metal lattice, H_2S can affect CO_2 corrosion by various other mechanisms. It has been reported that trace quantities of H_2S retard corrosion processes at ambient temperature due to formation of a protective FeS film by solid-state reaction¹⁴:



or by precipitation according to:



Depending on environmental factors, different thermodynamically stable types of FeS can be formed, as well as kinetically influenced intermediate phases. In some cases, FeS films can be non-protective and result in localized attack. For example, due to differences in density between the corrosion layer (potentially protective) and the base metal, the formed sulfide layer can generate internal stresses which can lead to film failure, resulting in sites for potential localized attack.

EXPERIMENTAL PROCEDURE

The experiments were performed in a large scale stainless steel flow loop, the so called “ H_2S system”, in order to simulate real field conditions. This system is comprised of 101.6 mm diameter, Sch 80, Hastelloy[®] C-276 (UNS No. 10276) for resistance to corrosion and stress corrosion cracking, two progressive cavity pumps (PCP) for conveying liquid and gas and three separate test sections for corrosion monitoring¹⁶. For the present work, only the downstream test section is used. In this section two coupons are flush-mounted at the top of the line while two others are similarly installed at the bottom. A system of coils is used for the cooling of the gaseous phase, allowing condensation to occur, as shown in Figure 1. The H_2S flow loop has a large Hastelloy[®] C-276 clad tank (1000 liters capacity) from where the liquid solution is drawn from the bottom using one of the progressive cavity pumps (PCP), while the other PCP is used to pump the gas/vapor mixture around the flow loop which is 41 m in length, creating a stratified two-phase flow regime.

This closed flow system is horizontal and is well insulated from the environment. Heat is added to the system using two resistance-heaters, which are immersed in the tank.

Liquid phase specification

The liquid phase is originally made up of de-ionized water and dissolved gases only, although dissolved ferrous iron build-up occurred throughout the test due to the corrosion process on the weight loss coupons. No salt or other chemicals were added. Liquid samples were regularly taken for analysis.

The pH of the liquid phase at the tank (bottom of the line) is kept at a value around pH 4~4.5 in each test and the solution is always under-saturated with regard to FeCO_3 . In the tests with H_2S , the solution was slightly supersaturated with regard to FeS .

Gas phase composition

In all the experiments, the gas phase comprised of a mixture of CO_2 and N_2 . For the H_2S environment, the required amount of H_2S was introduced in pure gaseous form at the beginning of the test and then checked and maintained regularly. The H_2S concentration was measured using colorimetric tubes, which give accurate readings of the H_2S concentration in the gas phase. Initially, the trace amounts of H_2S introduced in the loop were “consumed” by the system fairly rapidly; the H_2S partial pressure had to be adjusted regularly to maintain it at a reasonably stable value.

Condensation Rate

Tests in the absence of H_2S were done in different flow loops, which similar characteristics to the previously described H_2S system, with the exception of them being made of out 316 stainless steel and therefore being suitable only for sweet corrosion studies. In these “sweet systems”, the condensation rate was set by adjusting the cooling water flow through the coiling tube and the condensation rate was measured by collecting condensed liquid in a device installed at the end of the test section.

Due to the hazards associated with the H_2S gas, the condensation rate could be measured in the H_2S loop using the same previously described device. Thus, after setting the desired condensation rate in a sweet system, the temperature difference between the gas flow and the pipeline wall was accurately measured using thermistors. Considering that the temperature difference is the main driving force for the condensation to occur, the same temperature difference was set for the H_2S system in order to mimic the condensation rate in the H_2S loop.

Measurement Techniques

A weight loss technique was used to calculate the time and space averaged corrosion rate. Prior to exposure, each coupon was polished with 600 grain sand paper following the ASTM G 1 -81 Standard¹⁷, dehydrated with isopropyl alcohol, dried and weighed. After each experiment, coupons were removed from the system, their surface was immediately flushed with isopropyl alcohol to prevent oxidation and then dried. They were then weighed and pictures of the surface were taken for visual examination of the corrosion layer.

Scanning Electron Microscopy (SEM) was performed on selected coupons for analysis of the morphology of the corrosion layer; its elemental composition was determined by Energy Dispersive Spectrometry (EDS).

After removal of the corrosion layer, the weight loss for each specimen was determined and the corrosion rate was calculated. The carbon steel coupons used to measure the corrosion rate were flat surface disks; only one face of the coupon was in direct contact with the corrosive environment. The other faces were coated with Teflon to avoid electrical contact with the probe holders or with the environment. In Figure 2 the appearance of a typical weight loss coupon used in this project is shown. The coupons are shown as they were prior to exposure and after polishing. The coupons have a 3.14 cm external diameter and 0.757 cm diameter hole in the center. They were made from API 5L X-65 carbon steel, with a chemical composition shown in Table 1.

TEST MATRIX

The test matrix is divided into two different experimental series. The temperature, gas velocity and condensation rate were kept constant for all the experiments. The total pressure was fixed at 3 bars, the temperature was set at 70°C, and the condensation rate was 0.25 ml/m²/s, while the superficial gas velocity was 5 m/s. The pH was monitored as fixed by the experimental conditions¹⁸.

Series I

The first series (Series I) aims at studying the effect of the H₂S partial pressure (pH₂S) on TLC, where different pH₂S values were tested (0 to 0.13 bars). In this series the influence of CO₂ partial pressure (pCO₂) and pH₂S is studied in four different experiments (I-3, I-4, I-5 and I-6). The effect of pCO₂ was evaluated in two steps, changing it from 0.13 bars to 1.3 bars, while the total pressure was maintained at 3 bars by addition of nitrogen. The test duration was two days, each experiment was repeated twice. Table 2 shows details of the experimental conditions for Series I.

Series II

Series II consists of variable duration experiments where the influence of H₂S and CO₂ are studied. As in Series I, these experiments aim at studying the effect of the pH₂S on TLC but at longer times. Different pH₂S were tested from 0 to 0.13 bars. In this series the influence of H₂S partial pressure (pH₂S) is studied in four different experiments, including the baseline experiment with no H₂S and experiments with 0.004 bars, 0.07 bars and a 0.13 pH₂S. Experiments of 2, 7, 14 and 21 days duration were done in order to investigate the development of the corrosion layer and possible changes in its protectiveness. Details of Series II experimental conditions are shown in Table 3.

RESULTS

Corrosion rate

For reasons of confidentiality, the corrosion rates shown in the attached figures are normalized (the corrosion rate values are divided by an arbitrary constant). The numbers shown next to each data point represent the number of coupons used to calculate the average corrosion rate. The error bars correspond to the maximum and minimum values obtained after the weight loss measurement. No bottom-of-the-line results are presented in this paper; the reader is invited to check the source document¹⁸ for a detailed discussion of these data.

Figure 3 shows results related to the influence of $p\text{H}_2\text{S}$. Compared to a pure CO_2 environment, the introduction of 0.004 bar of H_2S decreases the average corrosion rate at the top of the line by 65%. When the $p\text{H}_2\text{S}$ increases to 0.013 bar, the downward trend continues with a corrosion rate approaching very low values. However, when the partial pressure of H_2S is further increased to 0.07 bars, the trend is reversed as the CR increases. Further increase of the $p\text{H}_2\text{S}$ to 0.13 bars does not seem to have a clear effect on the top of the line CR which remains at a similar value as measured at 0.07 bars of H_2S .

Figure 4 presents the influence of the $p\text{CO}_2$ at the top of the line. It is seen that the top of the line corrosion rate almost doubles if the $p\text{CO}_2$ is increased by an order of magnitude (from 0.13 bars to 1.3 bars) independently of the $p\text{H}_2\text{S}$.

For the variable duration test (Series II), the corrosion rates results are displayed in two different graphs. The first graph (Figure 5) shows the corrosion rate as calculated by weight loss, while the second one (Figure 6) shows the *differential corrosion rate* that is obtained as the cumulative effect of the corrosion damage from previous days is subtracted.

In most cases shown for Series II, a single coupon was used to calculate the corrosion rate, thus, no error bars are presented. As previously discussed, trace amounts of H_2S retard the general corrosion rate in short-term experiments, as can be seen in Figure 5 with a average corrosion rate in presence of H_2S at least two times lower than in pure CO_2 . This is generally explained by the solid state reaction (6) which results in formation of a protective FeS film at the surface of the metal. Further addition of H_2S seems to cause a gradual increase in the corrosion rate even is it is difficult to identify a distinct trend. In contrast to pure CO_2 conditions, the corrosion rate in the presence of H_2S decreased rapidly in the first 15 days and then reversed this trend and increases slightly (at any partial pressure of H_2S tested here). Another difference, compared to a pure CO_2 environment, is that in the presence of H_2S the corrosion rate did not decrease to very low values in long exposures as can be seen in Figure 6. There very low pure CO_2 corrosion rates are measured after 18 days of experimentation while the addition of trace amounts of H_2S retarded the initial corrosion rate but the corrosion rate remained rather constant for the entire duration of the experiment.

Surface Analysis

The surface appearance of the coupons was recorded immediately after their removal from the test loop. Photographs of the surface of the coupons are presented in Figure 7. In all cases, the layer seen there has similarities. Round surface features which are related to the presence of droplets of condensed liquid are seen on the surface of the coupons. The rounded shapes are more and more evident as the test duration increases. It is mainly due to the fact that, as the duration of the test increases, the droplet is likely to form on the same place over and over again (localized condensation). The corrosion product film that forms may also be changing the surface tension, thus affecting the residence time of the droplets.

Figure 8 and Figure 9 present SEM pictures and EDS analysis of the corrosion product layer present on the surface of the top of the line coupons in pure CO_2 environment for respectively the 2, 7 14 and 21 days experiments without any H_2S

present (Experiment II-0). The pictures show many common characteristics: a corrosion product layer almost exclusively formed of a dense FeCO_3 phase (see Figure 9). For the experiments without H_2S , initiation of localized corrosion could be observed after 14 days of testing. A few pits were identified on the surface of the coupons after 14 and 21 days of experiment as it can be inferred by looking at Figure 8. The corrosion product layer was removed and the presence of localized attack was verified (Figure 10 and 11).

Although the pCO_2 was 2 bar, no FeCO_3 crystals could be seen in the layer formed in the mixed $\text{CO}_2/\text{H}_2\text{S}$ environments (see Figures 12 to 17). Instead, a different mostly amorphous and fairly homogenous corrosion product layer is seen on the surface of the coupons. The EDS analysis presented in Figures 13, 15 and 17 show the presence of sulfur and iron but does not indicate the presence of FeCO_3 . At the border of a wetted/non-wetted area, both EDS and backscatter analysis were used to better define the regions. No difference could be seen in the composition of the surface layer. The corrosion layer formed on the coupons exposed to the $\text{CO}_2/\text{H}_2\text{S}$ environment for 21 days was removed and the surface analyzed. In all cases, the steel surface was uniformly corroded and there was no trace of localized corrosion even after 21 days of test

CONCLUSIONS

- In pure CO_2 environments tested here, a FeCO_3 corrosion layer formed at the top of the line, what led to a steady decrease of the general corrosion rate in long exposures. However, clear indications of localized attack initiation were revealed at the top of the line after 14 days of experiment in pure CO_2 environments.
- In mixed $\text{CO}_2 / \text{H}_2\text{S}$ used in this study, the H_2S initially retarded the general corrosion rate at the top of the line by leading to formation of a FeS film probably through a solid state reaction. However the corrosion rate did not diminish much over time even after 21 days of experimentation. Whenever H_2S was presented (even in very small amounts), it was always found that, regardless of the value of pCO_2 , the corrosion layer film composition was predominantly FeS , as analyzed by EDS. No traces of localized attack could be found in these experiments under any of the $\text{CO}_2 / \text{H}_2\text{S}$ ratios tested.

REFERENCES

1. C. DE Waard and D. E. Milliams, Corrosion 31, 177 (1975).
2. L. Gray, B. Anderson, M. Danysh and P. Tremaine, "Mechanisms of Carbon Steel Corrosion in Brines Containing Dissolved Carbon Dioxide at pH 4", Corrosion 89, Paper 464, (New Orleans, LA; NACE 1989).
3. S. Nesic, J. Postlethwaite and S. Olsen, Corrosion 52, 280 (1996).
4. M. B. Kermani and A. Morshed, Corrosion 59, 659 (2003).
5. Y. M. Gunaltun, D. Supriyatman and J. Jumaludin, "Top of Line Corrosion in Multiphase Gas Lines: A Case History", Corrosion 99, Paper 36, (Houston, TX; NACE 1999).
6. S. Olsen and A. Dugstad, "Corrosion under Dewing Conditions", Corrosion 91, Paper 472, (Houston, TX; NACE 1991).
7. Y. M. Gunaltun and D. Larrey, "Correlation of Cases of Top of the Line Corrosion with Calculated Water Condensation Rates", Corrosion 00, Paper 71, (Houston, TX; NACE 2000).
8. B. Pots and E Hendriksen, "CO₂ Corrosion under Scaling Conditions – The Special Case of Top-of-the-Line Corrosion in Wet Gas Pipelines", Corrosion 00, Paper 31, (Houston, TX; NACE 2000).
9. E. Van Hunnik, B. Pots and E. Hendriksen, "The Formation of Protective FeCO₃ Corrosion Product Layers in CO₂ Corrosion", Corrosion 96, Paper 5278, (Houston, TX; NACE 1996).
10. F. Vitse, K. Alam, Y. Gunaltun, D. Larrey and P. Duchet-Sucaux, "Semi-Empirical Model for Prediction of the Top-of-the-Line Corrosion Risk", Corrosion 02, Paper 2245, (Houston, TX; NACE 2002).
11. F. Vitse, S. Nesic, Y. Gunaltun, D. Larrey and P. Duchet-Sucaux, "Mechanistic Model for the Prediction of Top-of-the-Line-Corrosion Risk", Corrosion 03, Paper 3633, (San Diego, CA; NACE 03).
12. B. Brown, K-L. J. Lee, S. Nesic, "Corrosion in Multiphase Flow Containing Small Amounts of H₂S", Corrosion 03, Paper 3341, (San Diego, CA; NACE 2003)
13. S. Nesic, K-L. J. Lee, Corrosion 59, 616 (2003).
14. Ikeda, A., Ueda, M., and Mukai, S., "Influence of Environmental Factors on corrosion in CO₂ Source Well", Advances in CO₂ Corrosion, Vol. 2, 1985.
15. B. Pots et al, "Improvements on de-Waard Milliams Corrosion Prediction and Applications to Corrosion Management", Corrosion 02, Paper 2235, (Houston, TX; NACE 2002).
16. B. Brown and A. Schubert, "The Design and Development of a Large-Scale, Multiphase Flow Loop for the Study of Corrosion in Sour Gas Environments", Corrosion 02, Paper 2502, (Houston, TX; NACE 2002).
17. G. Haynes and R. Baboian, "Laboratory Corrosion Test and Standards", ASTM Special Technical Publication 866, p. 505, Philadelphia, PA, (1985).
18. Camacho A. "CO₂ Top of the Line Corrosion in the Presence of H₂S", Ohio University, Chemical Engineering Master Thesis. (Athens, OH, August 2006).

TABLES

Table 1. Chemical analysis of the carbon steels used in the experiments

| Element | X65 Composition (%) | API 5L X65 Standard (%) |
|---------|---------------------|-------------------------|
| C | 0.13 | < 0.26 |
| Mn | 1.16 | <1.40 |
| P | 0.009 | < 0.03 |
| S | 0.009 | < 0.03 |

Table 2. Test matrix. Series I. Short term TLC experiment

Common parameters:

Total pressure = 3 bar

Gas Temperature = 70°C

Condensation rate = 0.25 ml/m²/hr.

Gas velocity = 5 m/s

Test duration = 2 days

| Experiment # | I-0 | I-1 | I-2 | I-3 | I-4 | I-5 | I-6 |
|-------------------------|----------|------------------|-------|------------------------------------|------------------------------------|------------------------------------|------------------------------------|
| Investigating | Baseline | H ₂ S | | CO ₂ / H ₂ S | CO ₂ / H ₂ S | CO ₂ / H ₂ S | CO ₂ / H ₂ S |
| pCO ₂ (bar) | 0.13 | 0.13 | 0.13 | 0.13 | 0.13 | 1.3 | 1.3 |
| pH ₂ S (bar) | 0 | 0.004 | 0.013 | 0.07 | 0.13 | 0.07 | 0.13 |

Table 3 Test matrix. Series II. Variable duration TLC experiment

Common parameters:

Total pressure = 3 bar

Gas Temperature = 70°C

Condensation rate = 0.25 ml/m²/hr.

Gas velocity = 5 m/s

Test duration = 21 days

| Experiment # | II-0 | II-1 | II-2 | II-3 |
|-------------------------|----------|------------------|------|------|
| Investigating | Baseline | H ₂ S | | |
| pCO ₂ (bar) | 2 | 2 | 2 | 2 |
| pH ₂ S (bar) | 0 | 0.004 | 0.07 | 0.13 |

FIGURES



Figure 1: Test section of the H₂S loop

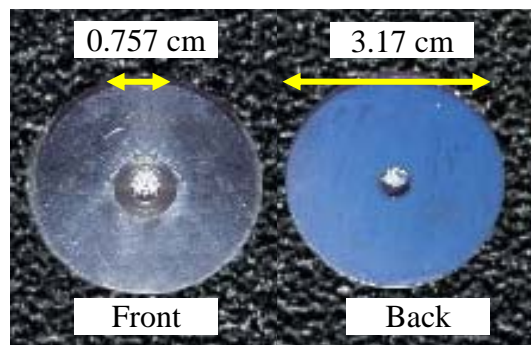


Figure 2. Weight loss coupons with Teflon coating at the back and the side (External diameter = 3.14 cm, Internal diameter 0.757 cm)

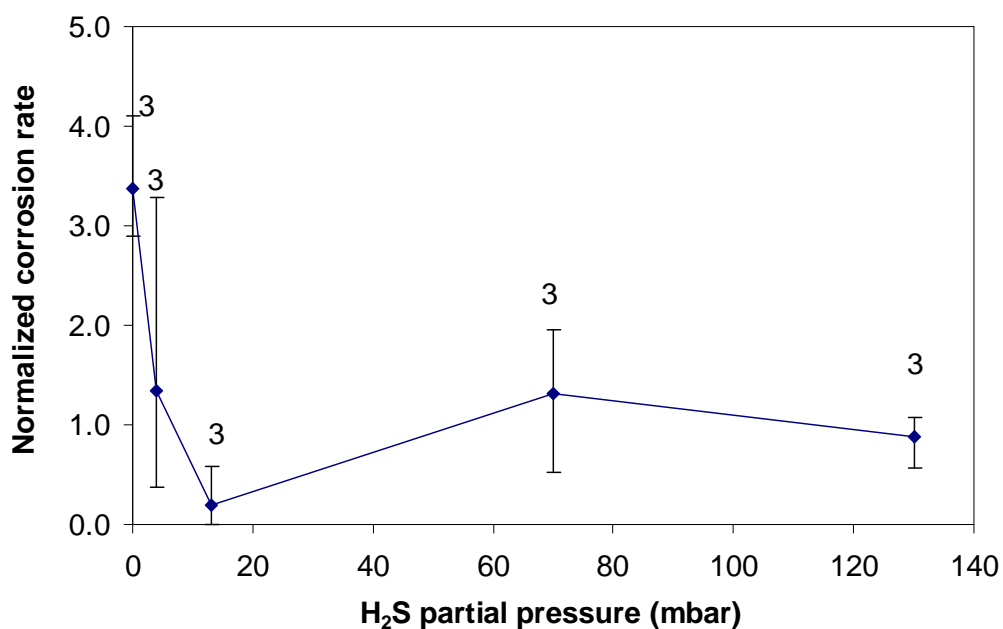


Figure 3. Series I. Effect of the H₂S partial pressure at the top of the line.
T = 70°C, P = 3 bars, pCO₂ = 130 mbar, V_G = 5 m/s, condensation rate = 0.25 ml/m²/s.

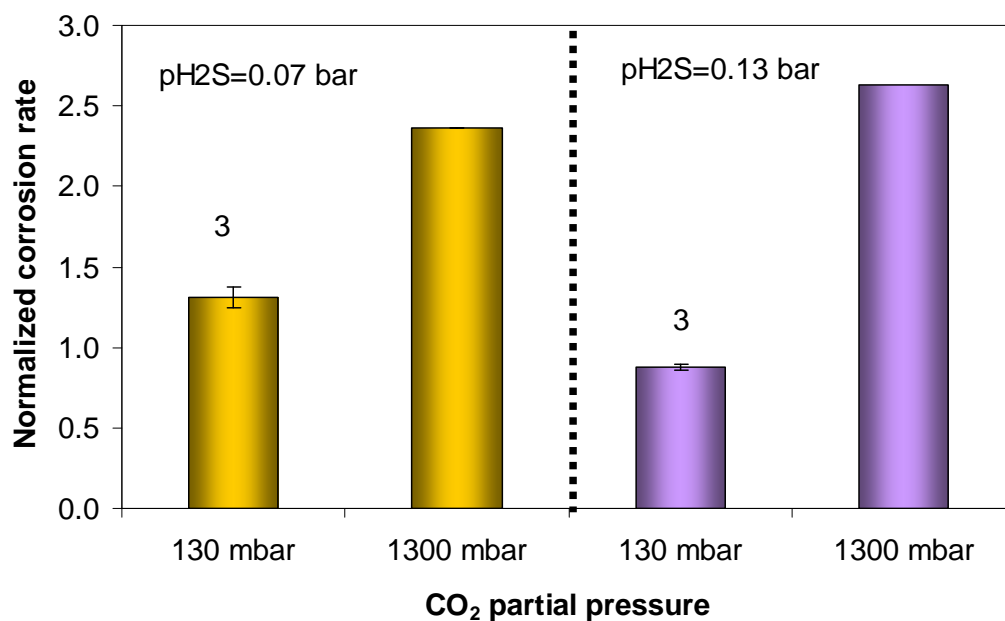


Figure 4. Series I. Effect of the CO₂ partial pressure at the top of the line. T = 70°C, P = 3 bars, V_G = 5 m/s, condensation rate = 0.25 ml/m²/s

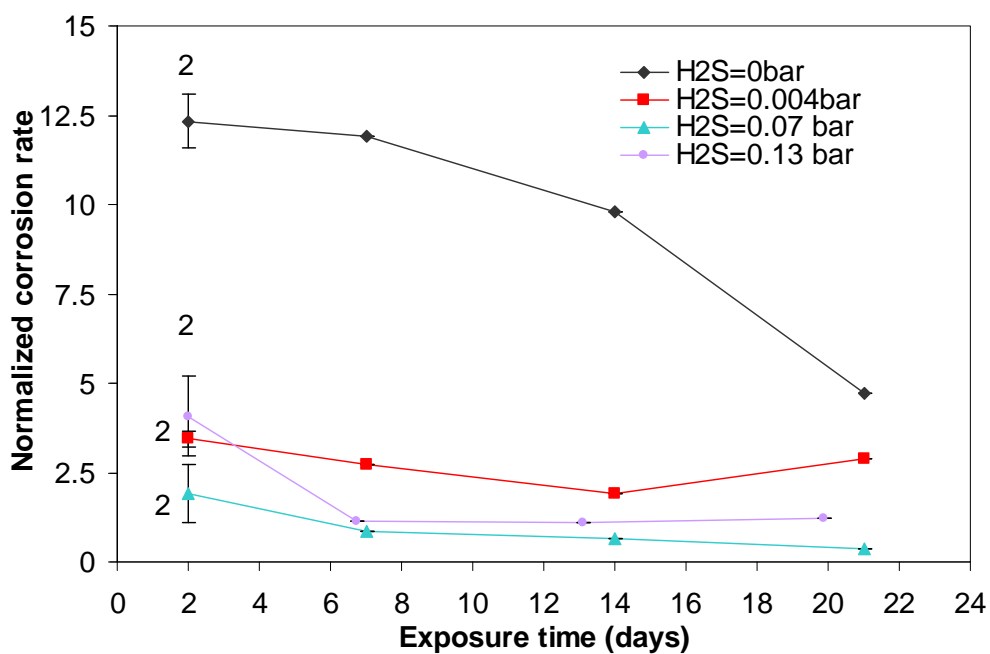


Figure 5. Series II, Effect of the H₂S concentration at the top of the line. 70°C, P = 3 bars, pCO₂ = 2 bars, V_G = 5 m/s, condensation rate = 0.25 ml/m²/s.

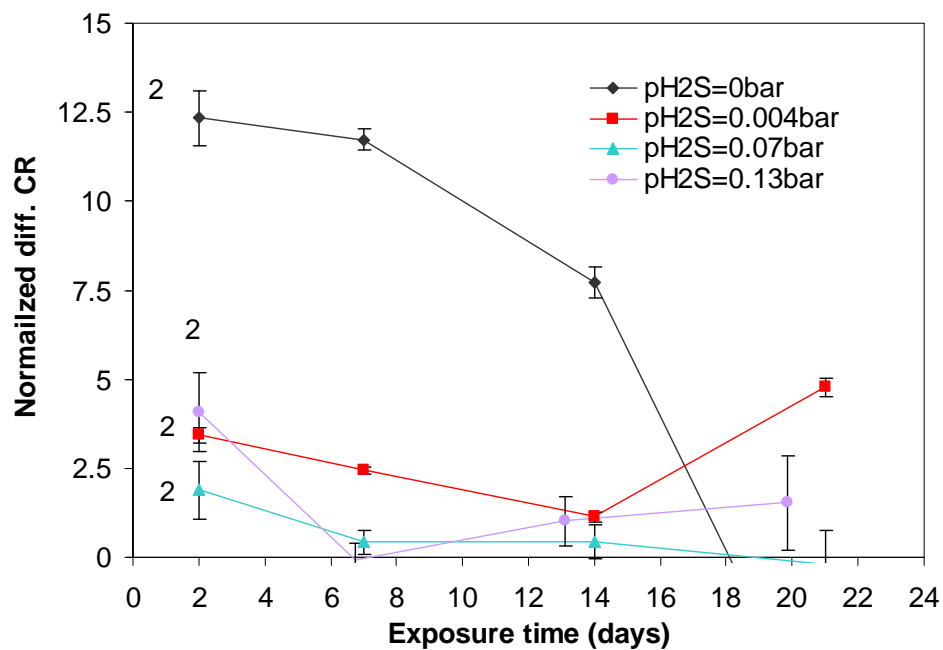


Figure 6. Series II, Differential corrosion rate. Effect of the H₂S concentration at the top of the line. 70°C, P = 3 bars, pCO₂ = 2 bars, V_G = 5 m/s, condensation rate = 0.25 ml/m²/s.

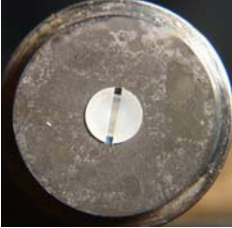



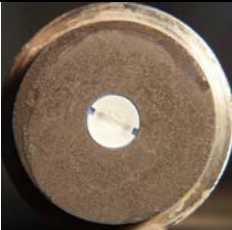



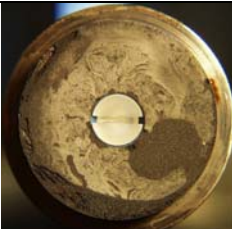



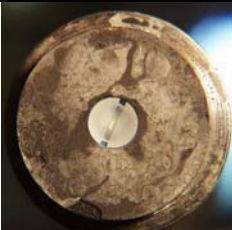



| | pCO₂ = 20. pH₂S = 1.3 (Top of the line) | | | |
|----------------|---|---|--|---|
| | No H₂S | 0.004 bar H₂S | 0.07 bar H₂S | 0.13 bar H₂S |
| 2 days |  |  |  |  |
| 7 days |  |  |  |  |
| 14 days |  |  |  |  |
| 21 days |  |  |  |  |

Figure 7. Series II. Morphology of carbon steel API X-65 coupons immediately after removal from the loop, tested at the top of the line. 70°C, P = 3 bars, pCO₂ = 2 bars, V_G = 5 m/s, condensation rate = 0.25 ml/m²/s

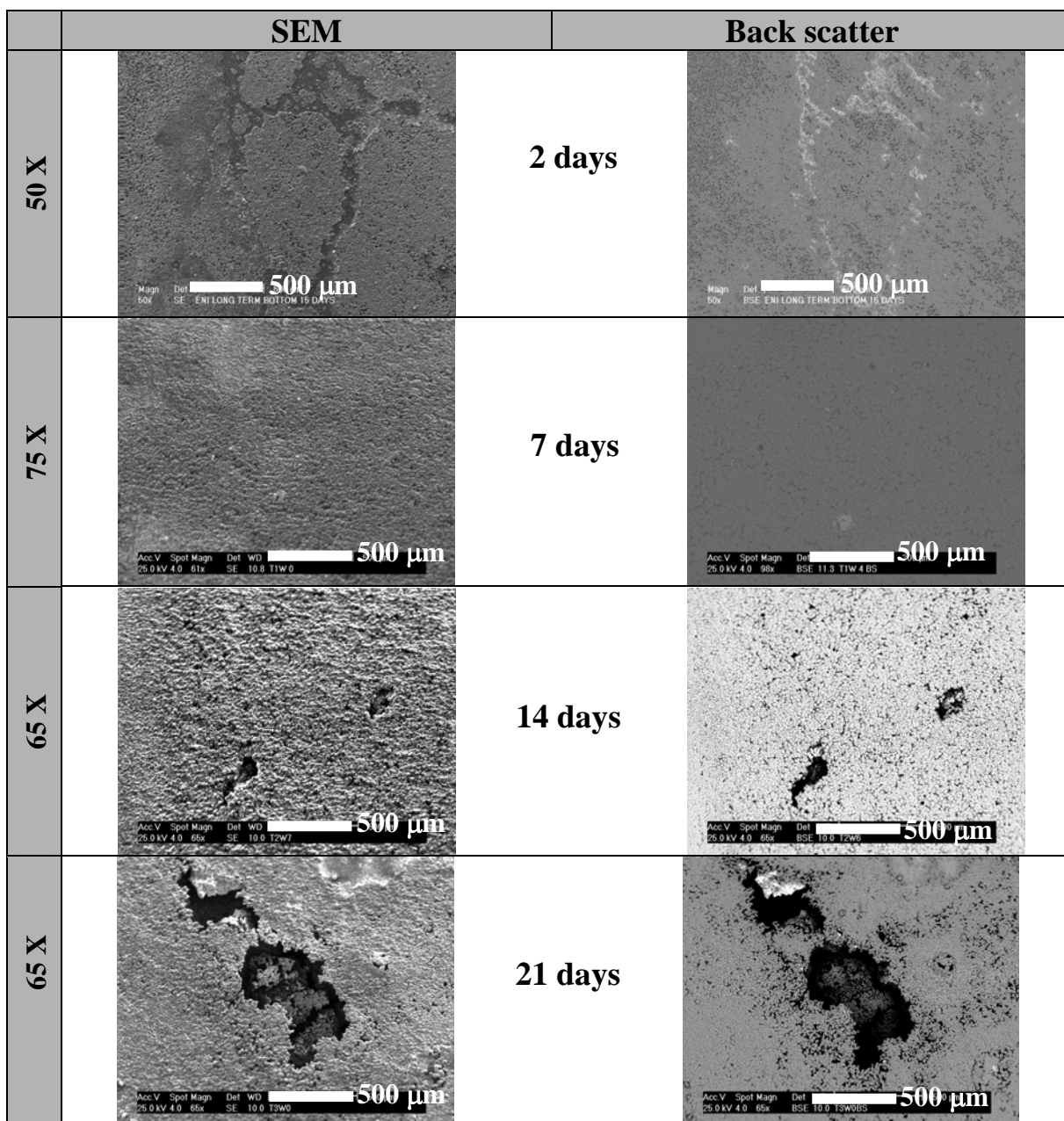


Figure 8. Experiment II-0. SEM and Backscatter images.
Top of the line. 70°C, P = 3 bars, pCO₂ = 2 bars, pH₂S = 0 bars, V_G = 5 m/s,
condensation rate = 0.25 ml/m²/s

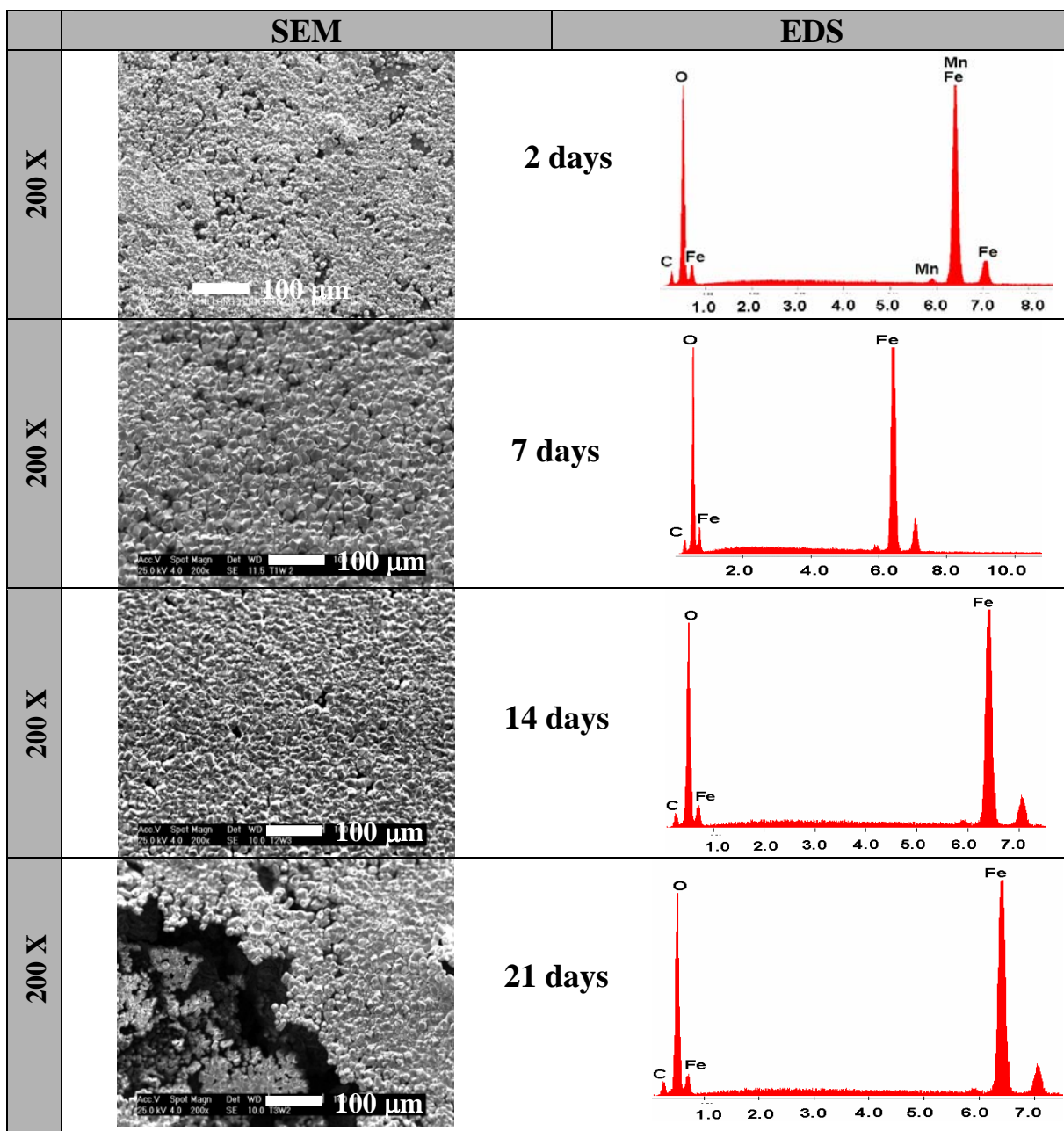


Figure 9. Experiment II-0. SEM and EDS analysis.
Top of the line. 70°C, P = 3 bars, pCO₂ = 2 bars, pH₂S = 0 bars, V_G = 5 m/s,
condensation rate = 0.25 ml/m²/s

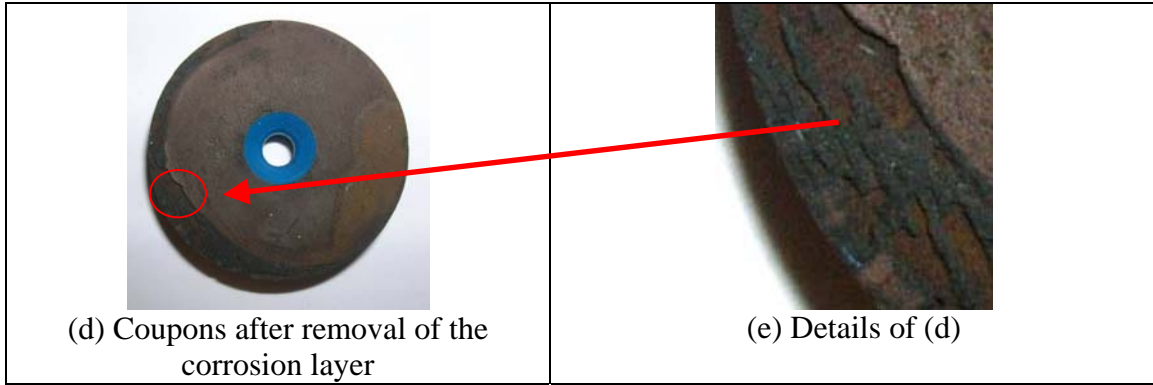


Figure 10. Experiment II-0. Coupon surface after 14 days of experiment. Top of the line. 70°C, P = 3 bars, pCO₂ = 2 bars, pH₂S = 0 bars, V_G = 5 m/s, condensation rate = 0.25 ml/m²/s

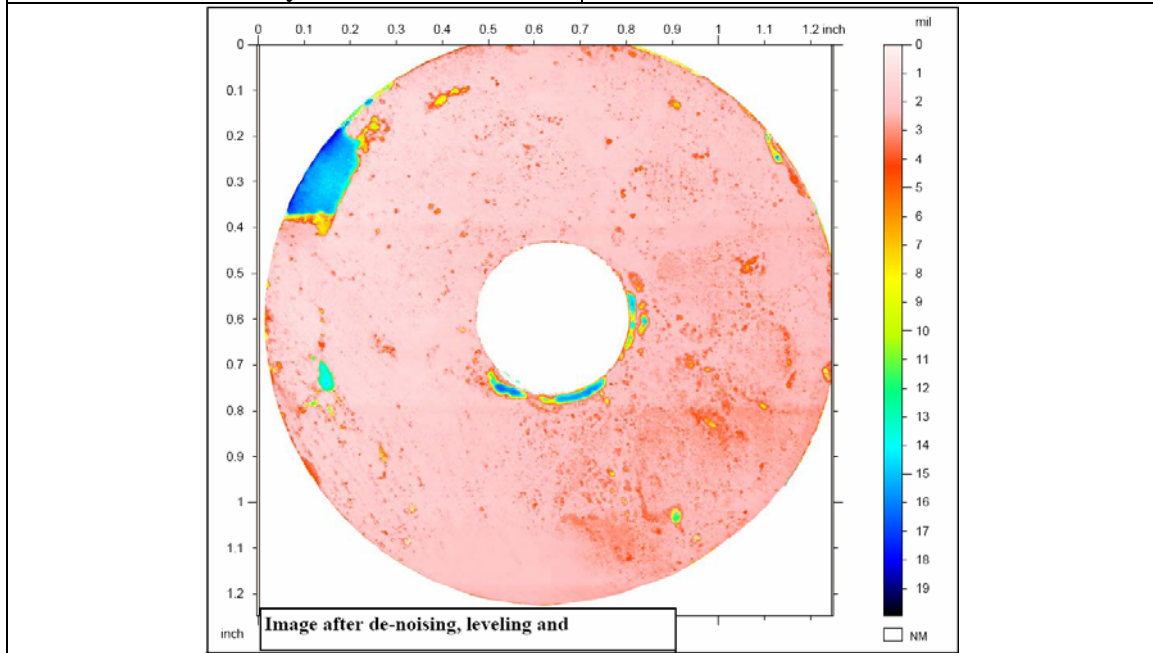
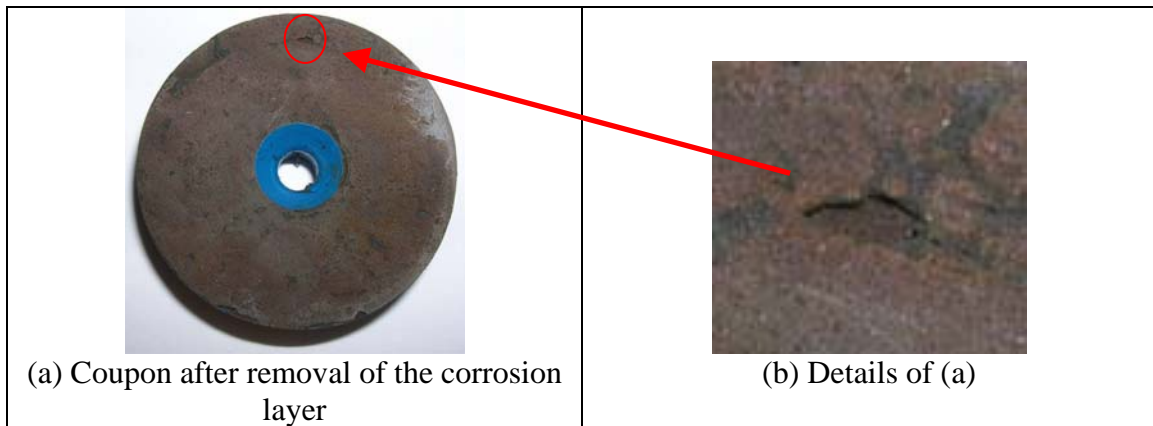


Figure 11. Experiment II-0. Coupon surface after 21 days of experiment. Top of the line. 70°C, P = 3 bars, pCO₂ = 2 bars, pH₂S = 0 bars, V_G = 5 m/s, Condensation rate = 0.25 ml/m²/s

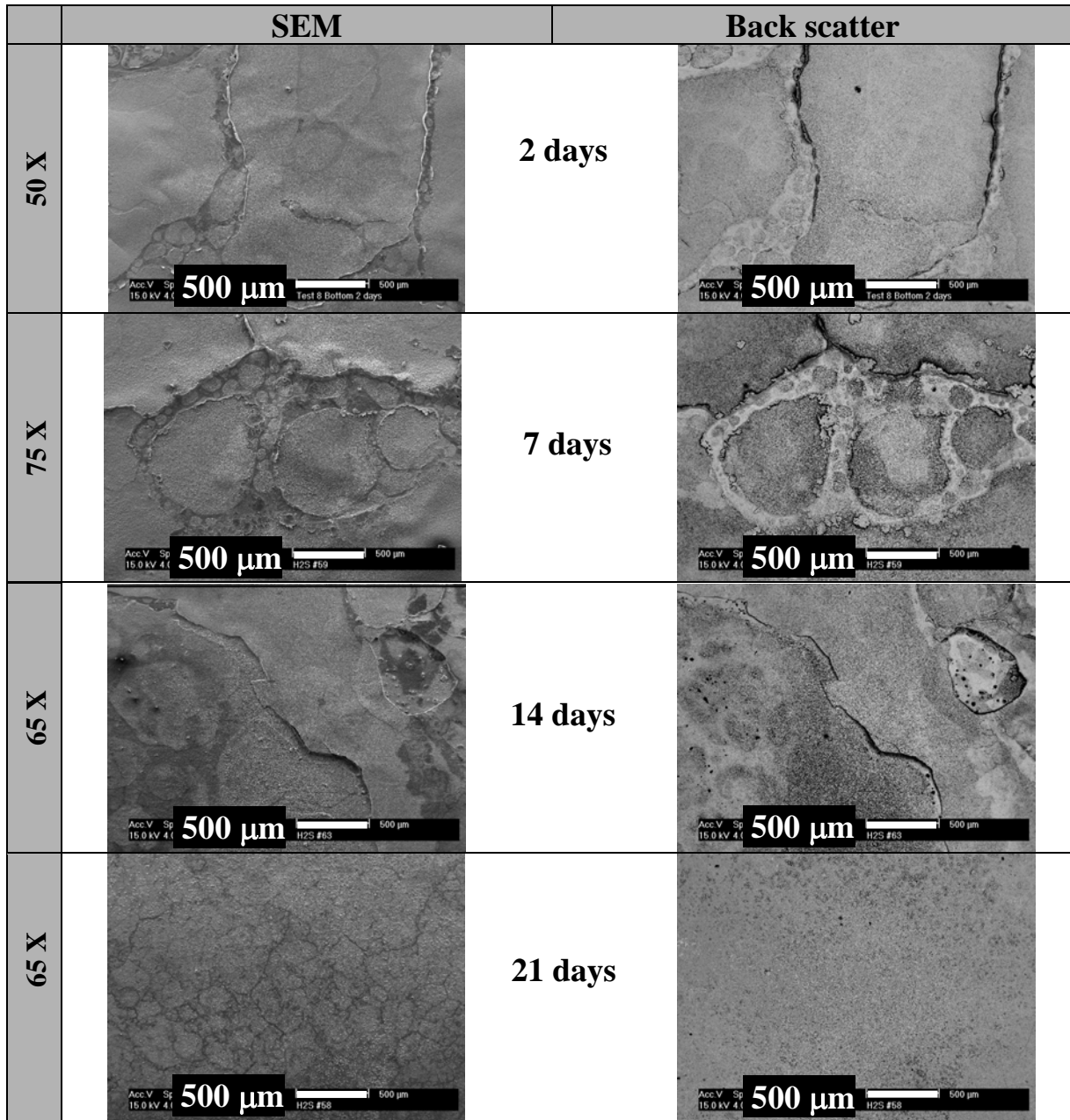


Figure 12. Experiment II-1. SEM and Backscatter images.
Top of the line. 70°C, P = 3 bars, pCO₂ = 2 bars, pH₂S = 0.004 bars, V_G = 5 m/s,
Condensation rate = 0.25 ml/m²/s

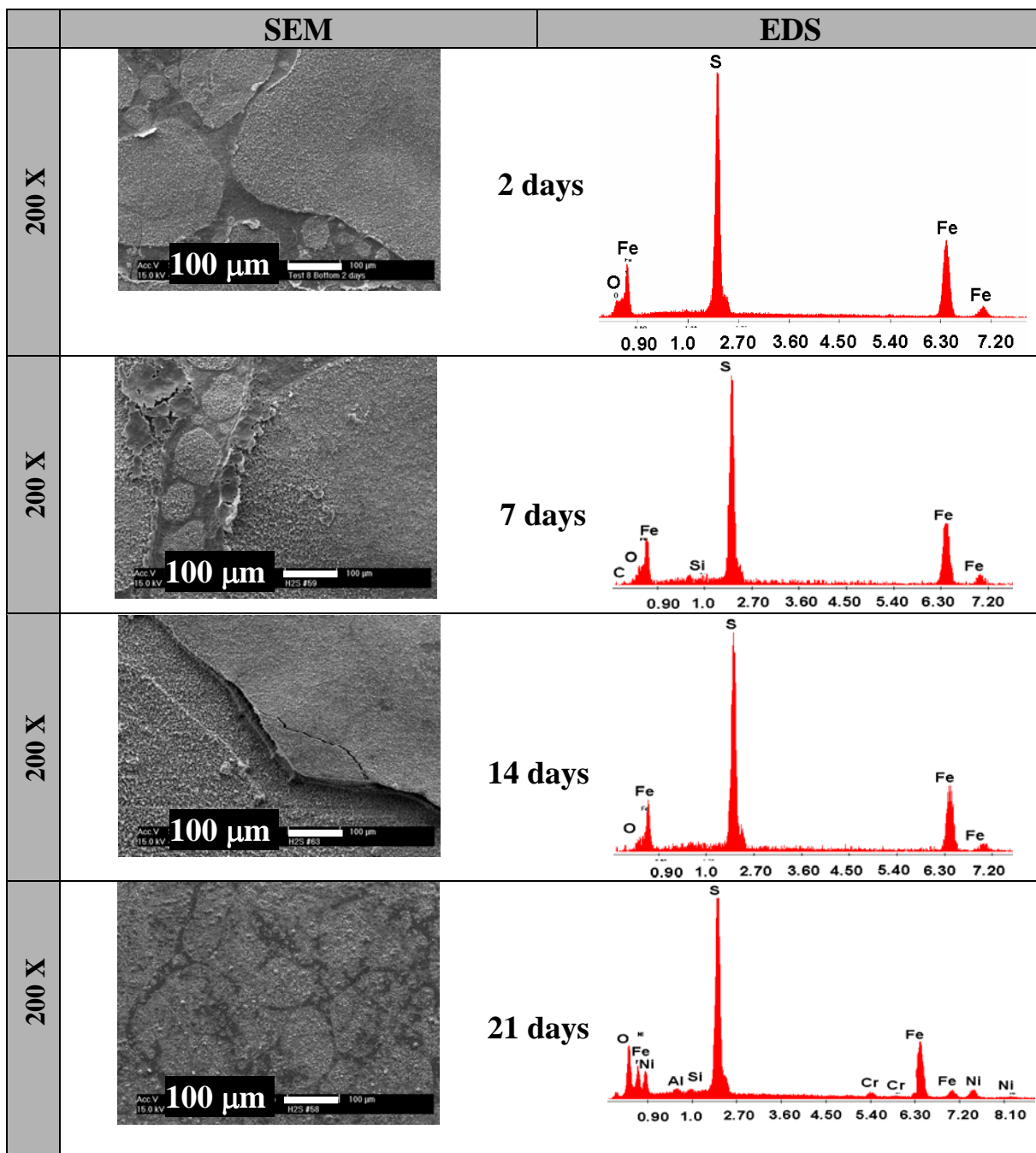


Figure 13. Experiment II-1. SEM and EDS analysis.
 Top of the line. 70°C, P = 3 bars, pCO₂ = 2 bars, pH₂S = 0.004 bars, V_G = 5 m/s,
 Condensation rate = 0.25 ml/m²/s

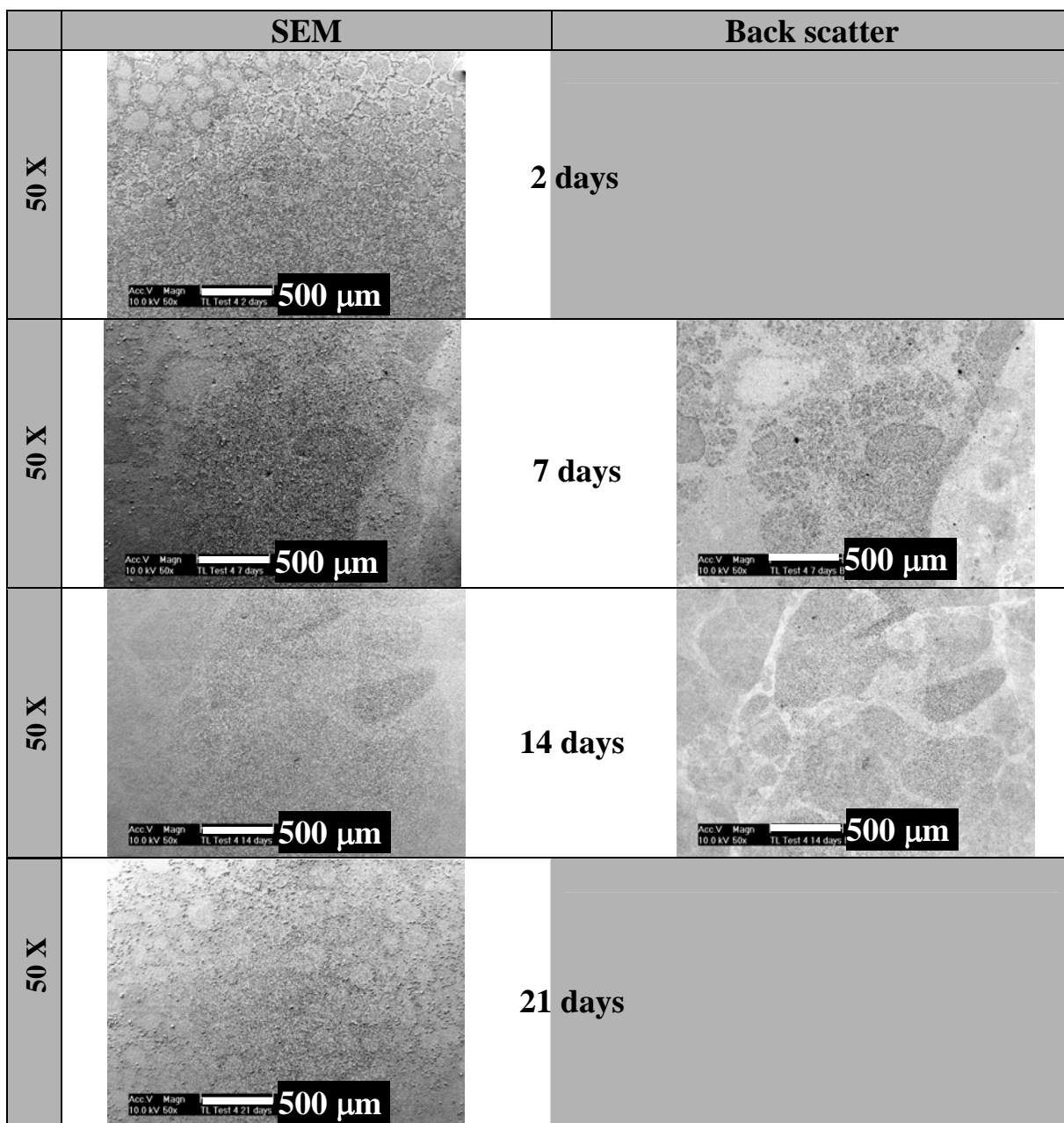


Figure 14. Experiment II-2. SEM and Backscatter images. Top of the line.
70°C, P = 3 bars, pCO₂ = 2 bars, pH₂S = 0.07 bars, V_G = 5 m/s,
Condensation rate = 0.25 ml/m²/s

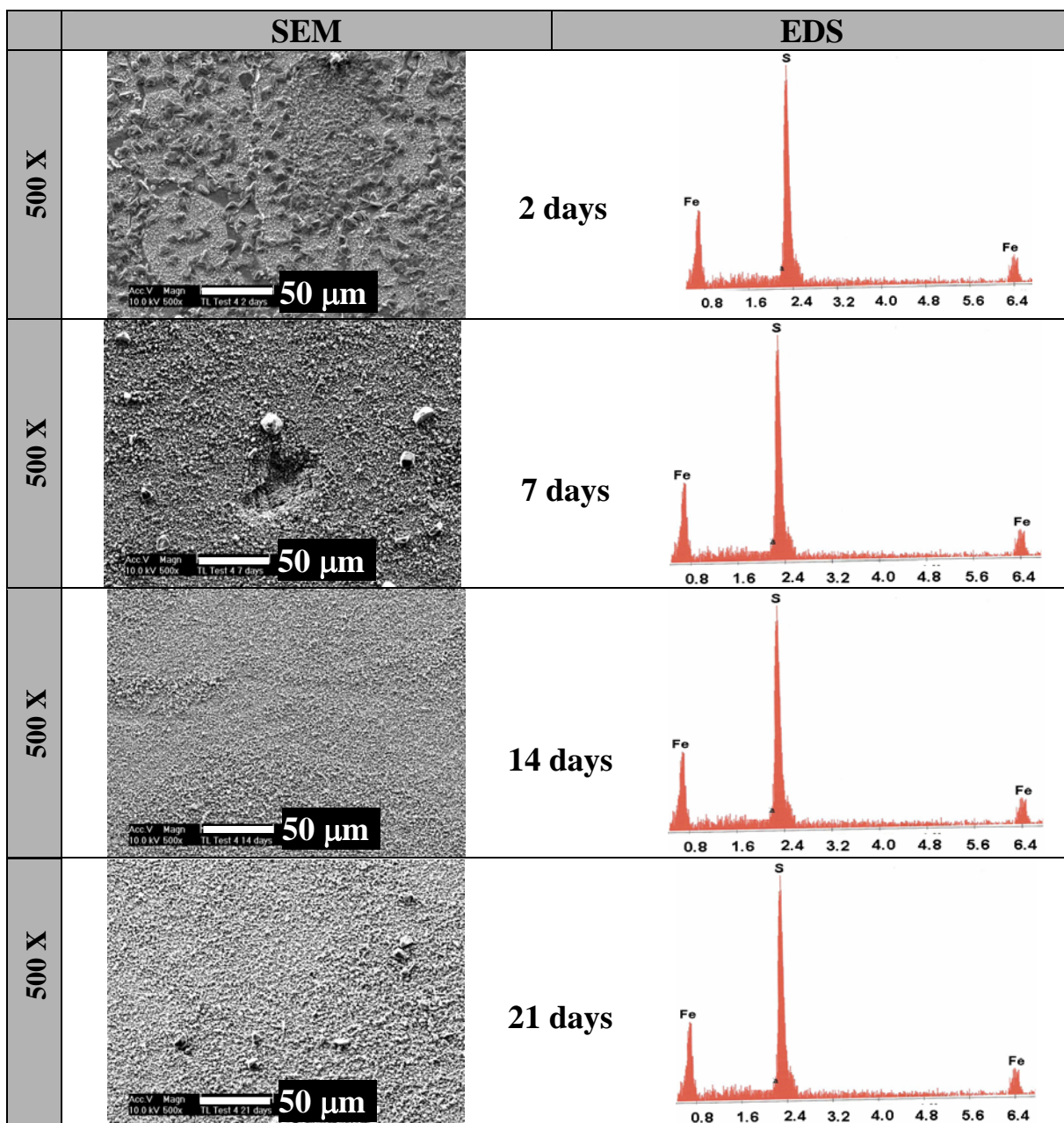


Figure 15. Experiment II-2. SEM and EDS analysis. Top of the line. 70°C, P = 3 bars, pCO₂ = 2 bars, pH₂S = 0.07 bars, V_G = 5 m/s, Condensation rate = 0.25 ml/m²/s

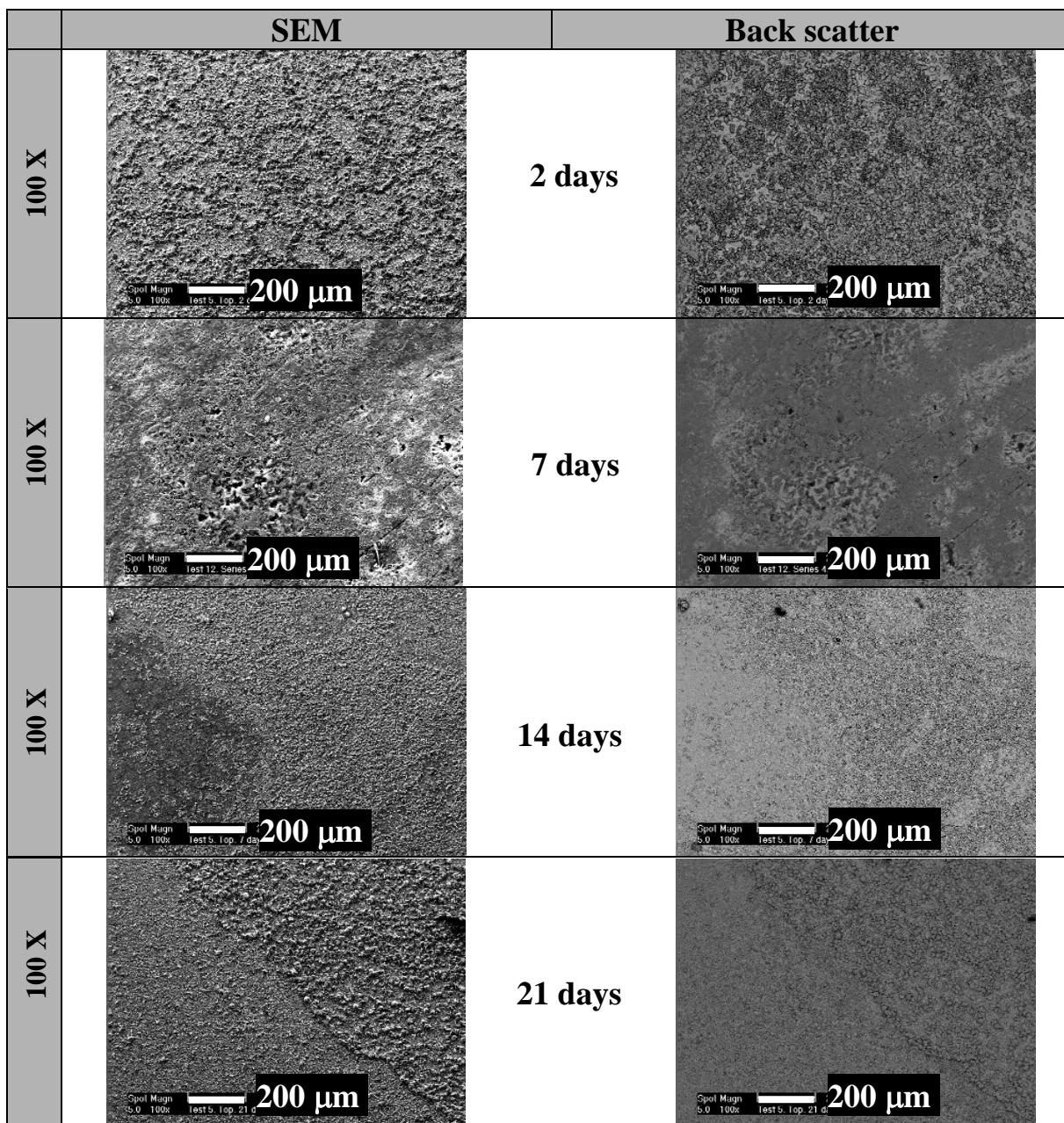


Figure 16. Experiment II-3. SEM and Backscatter images.
Top of the line. 70°C, P = 3 bars, pCO₂ = 2 bars, pH₂S = 0.13 bars, V_G = 5 m/s,
Condensation rate = 0.25 ml/m²/s

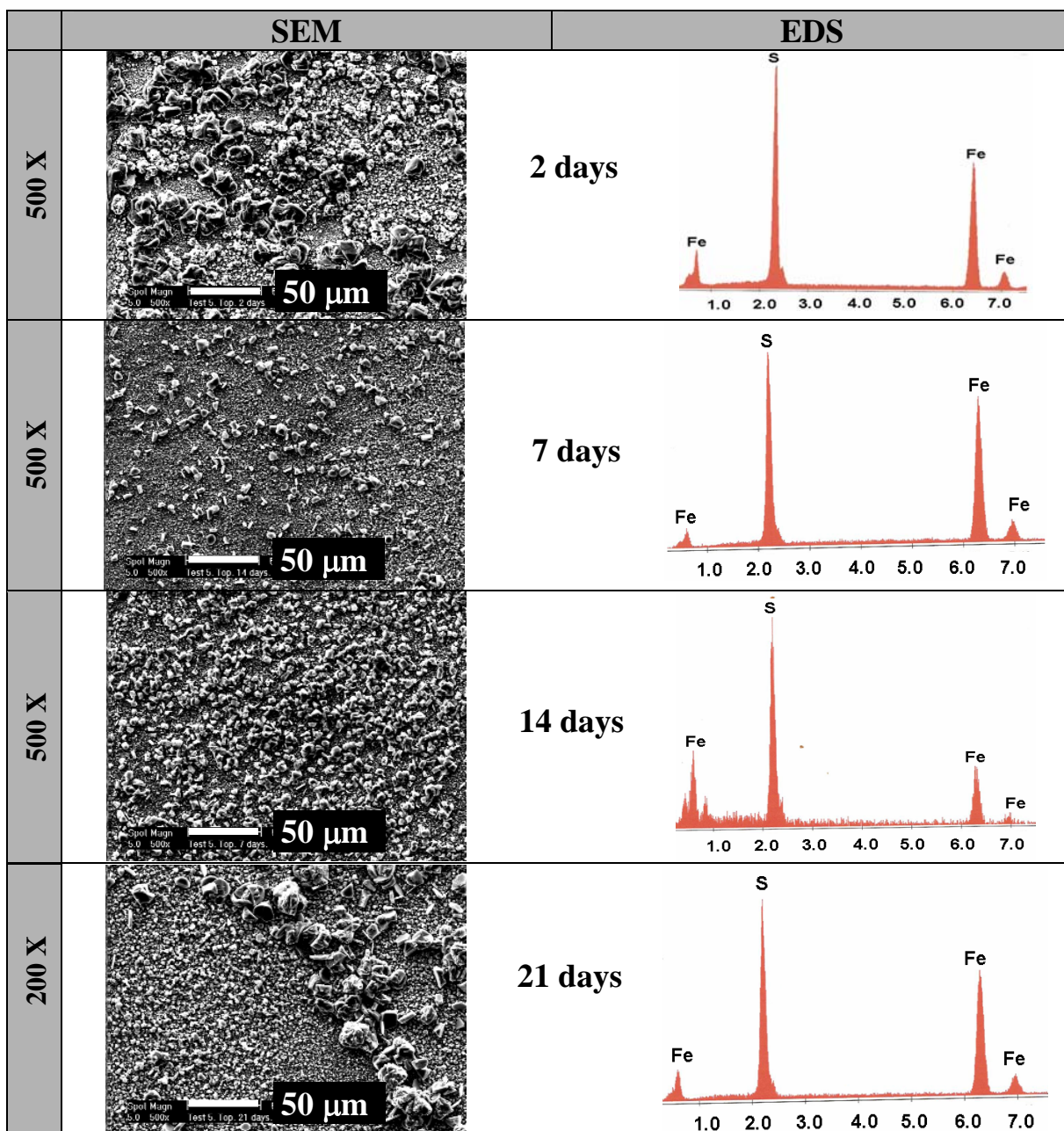


Figure 17. Experiment II-3. SEM and EDS analysis. Top of the line. 70°C, P = 3 bars, pCO₂ = 2 bars, pH₂S = 0.13 bars, V_G = 5 m/s, Condensation rate = 0.25 ml/m²/s